Time-Optimal Motion Control of Piezoelectric Actuator: STM Application

Yongkai Xu, Peter H. Meckl

Abstract—**This paper examines the problem of time-optimal motion control in the context of Scanning Tunneling Microscopy (STM) application and hysteresis compensation inherent to PZT actuators. The problem was divided into velocity tracking problem and point-to-point motion problem, and the time-optimal input profile was obtained using the command shaping technique of constrained least-square optimization. The optimal scanning velocity given a specific scanning distance and the effect of sampling rate have also been studied. To further improve the tracking performance, the piezoelectric hysteresis nonlinearity was modeled using the classical Preisach Model, and explicitly compensated using the proposed continuous numerical inversion algorithm.**

I. Introduction

Nanotechnology is currently a very active research area with a broad range of applications in materials science, computing, chemical and biological detection, and drug treatment. Scanning Tunneling Microscopy (STM) is a widely used tool to manipulate materials at the atomic level. By its nature, however, the probe/actuator system of a STM is inherently flexible and the induced vibration is the major limiting factor in achievable scanning precision and speed. Many researchers have addressed this problem in various ways. S. Devasia and co-workers [1]-[3] adopted a feedforward approach and proposed a model-based inversion method to achieve the minimum input energy. S. Salapaka et al. [4] and G. Schitter et al. [5] individually developed a controller based on H_∞ technique. X. Tan and J. S. Baras [6] proposed a robust control framework for smart actuators by combining inverse control with the l_1 robust control theory. C. J. Li et al. [7] designed a nonlinear piezo-actuator controller using a self-tuning regulator based on learning parameter estimation.

A typical scanning trajectory of STM consists of two parts: an active-scan region in which the probe scans at a precise velocity; and a transition region in which the probe goes back to the starting point in the x axis while the y axis is advanced to the next band as fast as possible [1], as shown in Fig. 1. The motion control problem is accordingly divided into a velocity tracking problem (control over the active-scan region) and a point-to-point motion problem (control over the transition region).

In this paper a time-optimal input profile is designed using the command shaping technique of constrained least-square optimization, which was first introduced by M. C. Reynolds and P. Meckl [8]. It enables the STM to accurately scan along the specified trajectory at a faster rate without exciting its vibrational mode.

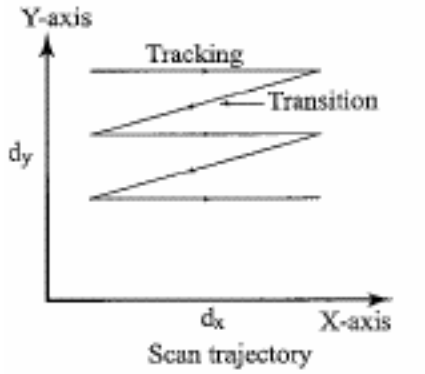

Fig. 1. Scanning trajectory (from [1])

Another major concern in STM application is hysteresis inherent to the piezoelectric actuator. Hysteresis is an input-output nonlinearity which, if left uncompensated, will degrade the system's overall performance. There are many ways to model hysteresis, but the most popular one is the classical Preisach model and its derivatives [9][10]. Though the Preisach model does not provide any physical insight into the problem, it can successfully produce behaviors very similar to physical systems.

A STM system can be modeled as the composition of a hysteresis nonlinear component H and a linear dynamic component G as shown in Fig. 2. Tao and Kokotovic [11] have shown that accurate position control is achievable if an inverse operator H^{-1} can be found such that H and H^{-1} "cancel" each other, thus allowing the controller to be designed based on the linear dynamics of the plant.

Many hysteresis inversion methods have been proposed.

Manuscript received September 22, 2003.

Yongkai Xu is with the School of Mechanical Engineering, Purdue University, West Lafayette, IN 47907 USA (phone: 765-494-6289; fax: 765-494-0539; e-mail: xuy@ purdue.edu).

Peter H. Meckl is with the School of Mechanical Engineering, Purdue University, West Lafayette, IN 47907 USA.

D. Hughes and J. T. Wen [12] utilized the monotonic nature of the first-order reversal curves (both the first-order descending curves and ascending curves) to invert the hysteresis function. R. Venkataraman and P. S. Krishnaprasad [13] proposed an inversion algorithm based on the contraction mapping principle by exploiting the properties of Lipschitz continuity and incrementally strict increase of the Preisach operator under some mild assumptions. X. Tan et al. [14] developed Closest Match Algorithm for the inversion directly based on a discretized hysteresis model.

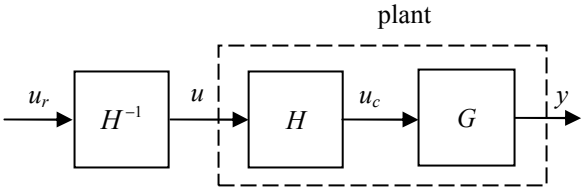

Fig. 2. Plant model

In this paper a continuous numerical inversion algorithm (CNIA) is proposed based on the classical Preisach Model and guaranteed to converge. The speed of convergence can be manipulated by choosing an appropriate stopping threshold. Simulations serve to demonstrate its effectiveness in attenuating the hysteresis nonlinearity.

II. TIME-OPTIMAL FEEDFORWARD DESIGN

A. Time-optimal command shaping

For now we focus on the x-axis movement because the actuator doesn't move in the y-axis during the active scanning period and therefore the y-axis movement doesn't affect the scanning accuracy. The x-axis reference trajectory (position reference and velocity reference, respectively) shown in Fig. 3 is divided into two parts.

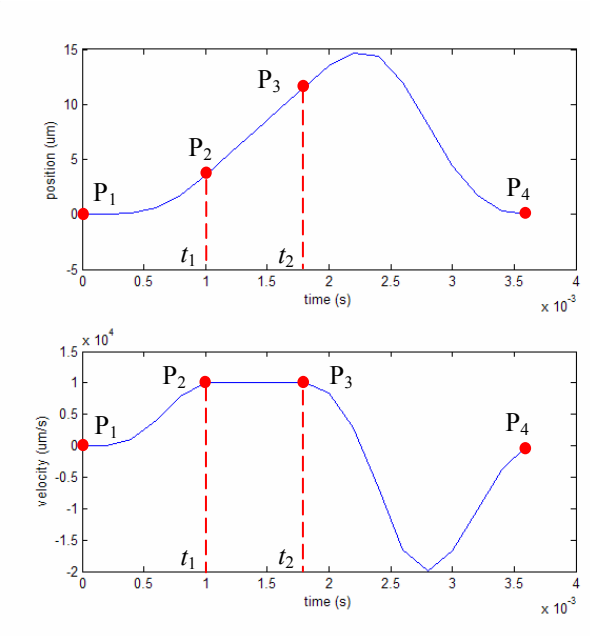

Fig. 3. Scanning reference trajectory.

The first part P_1P_3 is basically a velocity tracking problem. The scanning duration $T_{scan} = t_2 - t_1$ is determined by the specific scanning distance and velocity, thus t_1 is the optimization goal. By setting the tracking tolerance on P_1P_2 to infinity and the tracking tolerance on P_2P_3 to the desired value that meets the velocity tracking precision, the system is made to reach the desired velocity as fast as possible and then settle down to a nearly constant velocity for the duration of T_{scan}. The second part P_3P_4 is essentially a point-to-point motion problem without any tracking constraints, which enables the system to return to the starting point in the x-axis as fast as possible. This way the shaped command input will be time optimal.

The command shaping technique for tracking [8] is used to solve the optimization problem and can be formulated on the discrete-time state space representation as follows. Given the system

$$\begin{aligned} \mathbf{x}(k+1) &= \mathbf{A}\mathbf{x}(k) + \mathbf{B}u(k) \\ y(k) &= \mathbf{C}\mathbf{x}(k) \end{aligned} \tag{1}$$

we have

$$\mathbf{x}(k) = \mathbf{A}^k\mathbf{x}(0) + \mathbf{\Phi}\mathbf{U}(k) \tag{2}$$

where $\mathbf{\Phi} = [\mathbf{A}^{k-1}\mathbf{B} \quad \mathbf{A}^{k-2}\mathbf{B} \quad \cdots \quad \mathbf{B}]$, and

$\mathbf{U}(k) = [u(0) \quad u(1) \quad \cdots \quad u(k-1)]^T$.

The system output should satisfy the tracking tolerance:

$$\begin{aligned} y(k) &= \mathbf{C}\mathbf{x}(k) = \mathbf{C}\mathbf{A}^k\mathbf{x}(0) + \mathbf{C}\mathbf{\Phi}\mathbf{U}(k) \\ &\left| y(k) - y_d(k) \right| \le e_{allow}(k) \end{aligned} \tag{3}$$

If $y(k) - y_d(k) > 0$, (3) becomes

$$\mathbf{C}\mathbf{\Phi}\mathbf{U}(k) \le y_d(k) + e_{allow}(k) - \mathbf{C}\mathbf{A}^k\mathbf{x}(0) \tag{4}$$

Denote $\mathbf{R} = \mathbf{C}\mathbf{\Phi}$, $f_1 = y_d(k) + e_{allow}(k) - \mathbf{C}\mathbf{A}^k\mathbf{x}(0)$, (4) can be rewritten as

$$\mathbf{R}\mathbf{U} \le f_1 \tag{5}$$

For $y(k) - y_d(k) < 0$, we have a similar expression

$$-\mathbf{R}\mathbf{U} \le f_2 \tag{6}$$

where $f_2 = -y_d(k) + e_{allow}(k) + \mathbf{C}\mathbf{A}^k\mathbf{x}(0)$.

From (5) (6) we set up the tracking constraint for the k-th sampling instant as

$$\begin{bmatrix} \mathbf{R} \\ -\mathbf{R} \end{bmatrix} \mathbf{U}(k) \le \begin{bmatrix} f_1 \\ f_2 \end{bmatrix} \tag{7}$$

Also the actuator has a saturation limit:

$$|u(k)| \le F_{\max} \tag{8}$$

By incorporating the tracking constraint and actuator limit at each point on the trajectory in a least-square programming scheme, a time-optimal input profile can be obtained by increasing k until a solution satisfying the constraints results. The optimization problem is formulated as

$$\begin{aligned} &\min \quad \left\{ \left(\mathbf{x}(k)-\mathbf{x}_d\right)^T \left(\mathbf{x}(k)-\mathbf{x}_d\right) \right\}^{\frac{1}{2}}, \\ &\mathbf{U}(k) \\ &\text{subject to (7), (8)} \end{aligned} \tag{9}$$

There are many standard packages for solving linear least-square programming problems such as MATLAB. Compared to other optimization schemes, the largest advantage of this method is that tracking can be directly specified in the solution scheme, thus avoiding manipulating weighting factors that have little physical meaning.

The linear component G of STM model we used to do the simulation is a 4th-order transfer function (10) adopted from [1], which contains a pair of non-minimum phase (NMP) zeros at 1643 Hz and two vibration modes with natural frequencies of 241.9 Hz and 777.4 Hz, respectively.

$$G(s) = \frac{K\left(s^2 - 2\zeta_z\omega_z s + \omega_z^2\right)}{\prod_{i=1}^{2}\left(s^2 + 2\zeta_i\omega_i s + \omega_i^2\right)} \tag{10}$$

TABLE I
STM MODEL PARAMETERS

	Damping ratio	Natural frequency (Hz)
NMP zero	0.70	1643.0
1st mode	0.008	241.9
2nd mode	0.39	777.4
K	97000	

The resulting command profile is shown in Fig. 4. This profile doesn't have the symmetry shown in L. Y. Pao's work [15] and at the end of the maneuver the input doesn't go back to zero because the STM model doesn't have a rigid body mode. The position and velocity outputs for three cycles of the shaped time-optimal command are shown in Fig. 5.

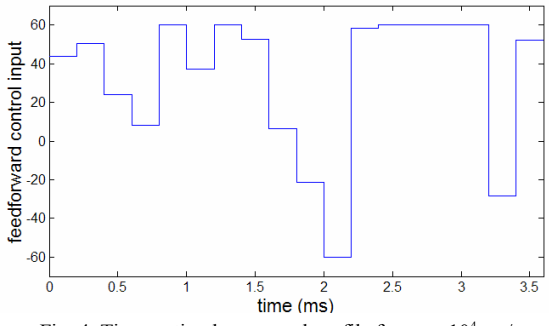

Fig. 4. Time-optimal command profile for $v_d = 10^4$ μm/s

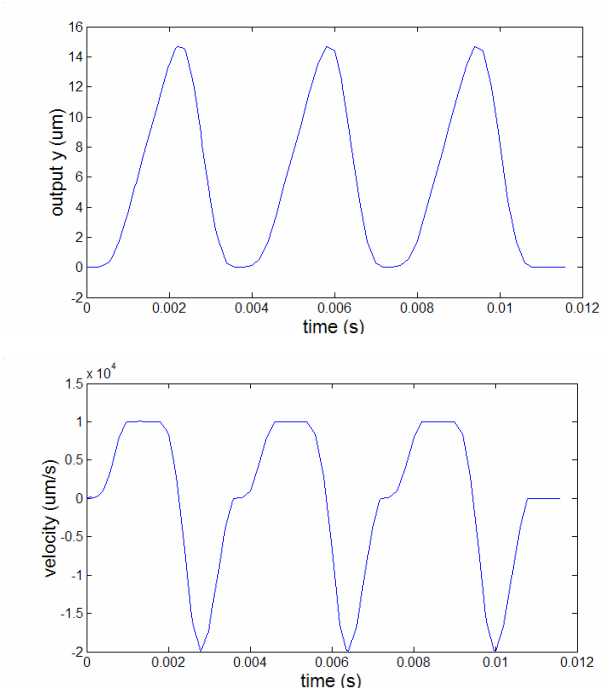

Fig. 5. Position and velocity outputs to the time-optimal command

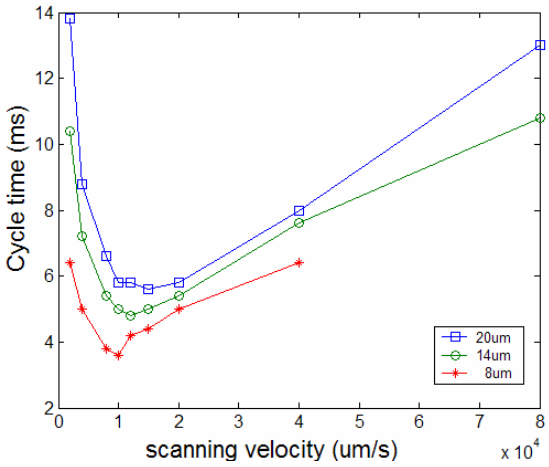

Fig. 6. Time optimality comparison between different scanning velocities

B. *Time optimality under different velocities*

The time optimality of the solution using different scanning velocities is investigated and the results are shown in Fig. 6 for three scanning distances of 20, 14 and 8 μm, respectively. It is observed that, for a given scanning distance, a higher scanning velocity does not necessarily result in a shorter cycle time because the time spent on the transition to reach the desired velocity may offset the time gained during the active scanning period T_{scan}. It is also

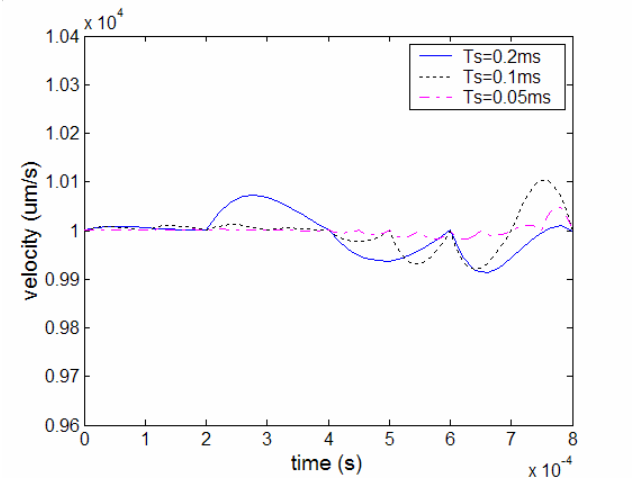

Fig. 7. The effect of sampling frequency on reducing the velocity tracking error

noticed that the optimal velocity v_d, for which cycle time is minimized, decreases when the scanning distance is reduced, for example, v_d for 20, 14 and 8 μm are 1.5, 1.2 and 1.0×10^4 μm/s, respectively.

The effect of the sampling rate on reducing velocity tracking error is also examined. The comparison of tracking errors in three cases (the sampling time of 0.2, 0.1 and 0.05 ms, respectively) is shown in Fig. 7, which is a zoom-in of the scanning portion (the desired scanning velocity is 10^4 μm/s). It can be observed that higher sampling frequency yields a feedforward profile with smaller velocity tracking error between two consecutive sampling instants.

III. Continuous Numerical Inversion of Hysteresis Nonlinearity

Like the Closest Match Algorithm (CMA) developed by X. Tan et al. [14], our proposed CNIA searches for the numerical approximation of the inverse hysteresis instead of trying to find the exact inversion. This significantly reduces the mathematical complexity of the inversion problem. The difference is that X. Tan's work was based on a discrete model of hysteresis while ours is essentially based on a continuous Preisach model.

The advantage from this difference can be illustrated with the analogy of numerical approximation of curves. CMA is like curve-fitting using a staircase profile (discrete approximation). The only way to reduce the approximation error is to refine the staircase, which means more experimental data have to be collected for the model identification, thus tremendously increasing the computational burden (they used least-square estimation). CNIA is like approximation using linear interpolation (hence we call it "continuous"), therefore much less identification data are needed without sacrificing the curve-fitting accuracy. Moreover, if the linear interpolation is replaced by higher-order polynomial fitting, which is easy to do, a further reduction in the approximation error can be expected.

The search method of CNIA yields a control input u^* that satisfies

$$\left|\hat{\Gamma}(u^*;\psi)-f_d\right|\le\varepsilon,\qquad u^*\in[u_{\min},u_{\max}] \tag{11}$$

where $\hat{\Gamma}$ is the Preisach operator of the identified hysteresis model, ψ is the input history, f_d is the desired hysteresis output and $\varepsilon>0$ is the allowed inversion error.

The algorithm is outlined as follows with an example of searching on a descending curve as illustrated in Fig. 8. We assume that the initial conditions of $u(0)$, $\psi(0)$ and the corresponding hysteresis ouput $f(0)=\hat{\Gamma}\left(u(0);\psi(0)\right)$ are given. The following iteration steps are for the k-th sampling instant ($k\ge1$). The notation $u^{(n)}(k)$ represents the n-th iteration value of $u(k)$. Without confusion, we drop the index k and only use $u^{(n)}$ to simplify the notation. u^* represents the returned value for $u(k)$ that satisfies (11). In addition to u^*, the algorithm also returns the updated input history ψ^* for the next sampling instant.

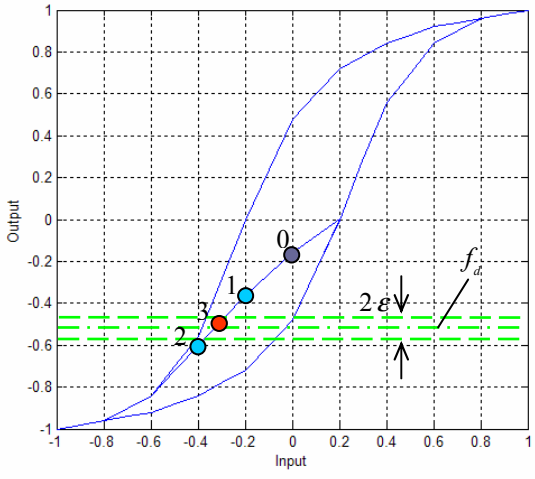

Fig. 8. Example of CNIA

Continuous Numerical Inversion Algorithm:

Step 1: Let $u^{(0)}=u(k-1)$, $\psi^{(0)}=\psi(k-1)$, and $f^{(0)}=f(k-1)$, as Point 0 in Fig. 8. Set iteration step $n=0$. If $f^{(0)}=f_d$, go to Step 5.

Step 2: Initialize the search step $\Delta u>0$. If $f^{(0)}>f_d$, it means that the desired hysteresis output is going down along a descending curve. Then let $u^{(1)}=u^{(0)}-\Delta u$ (this gives Point 1 in Fig. 8). Otherwise, if $f^{(0)}<f_d$, it means that the desired hysteresis output is going up

along an ascending curve. Then let $u^{(1)} = u^{(0)} + \Delta u$. And now $n = 1$.

Step 3: Saturation and Convergence check:

- Check if $u_{\min} \le u^{(n)} \le u_{\max}$. If not, let $u^{(n)} = u_{\min}$ if $u^{(n)} < u_{\min}$; let $u^{(n)} = u_{\max}$ if $u^{(n)} > u_{\max}$.
- Calculate the hysteresis output $f^{(n)} = \hat{\Gamma}\left(u^{(n)}; \psi^{(n-1)}\right)$; at the same time update the input history to $\psi^{(n)}$. If $\left|f^{(n)} - f_d\right| \le \varepsilon$ (as Point 3 in Fig. 8), the convergence has been reached. Go to step 5. Otherwise (as Point 1 and 2 in Fig 8) continue to next step.

Step 4: Modify the searching point:

- For the case of f_d being on a descending curve:
  - If $f^{(n)} - f_d > 0$, keep the current Δu as it is. Let $n = n+1$, $u^{(n)} = u^{(n-1)} - \Delta u$ (this gives Point 2 in Fig. 8). Go to step 3.
  - If $f^{(n)} - f_d < 0$, it means that the last increment of u is too large and the n-th test point has skipped over to the other side of f_d. Then reduce the increment by $\Delta u = \Delta u / 2$ and modify the n-th test point to $u^{(n)} = u^{(n-1)} + \Delta u$ (this gives Point 3 in Fig. 8). Go to step 3.
- For the case of f_d being on an ascending curve:
  - If $f^{(n)} - f_d < 0$, keep the current Δu as it is. Let $n = n+1$, $u^{(n)} = u^{(n-1)} + \Delta u$. Go to step 3.
  - If $f^{(n)} - f_d > 0$, it means that the last increment of u is too large and the n-th test point has skipped over to the other side of f_d. Then reduce the increment by $\Delta u = \Delta u / 2$ and modify the n-th test point to $u^{(n)} = u^{(n-1)} - \Delta u$. Go to step 3.

Step 5: Let $u^* = u^{(n)}$, $\psi^* = \psi^{(n)}$. Exit.

As each reversal curve (either ascending or descending) of the hysteresis is monotonic, the proposed search algorithm is guaranteed to converge. The number of iterations needed depends on the choice of the stopping threshold ε. Since the algorithm is implemented in a digital controller where A/D converters are used, the value of ε should not be smaller than the quantization error. CNIA outlined above uses the variant-step search algorithm, but other advanced search algorithms can be readily adopted.

The simulation result of open loop hysteresis compensation is shown in Fig. 9 and 10 which serve to demonstrate the effectiveness of CNIA in attenuating hysteresis nonlinearity. The notation of u, u_r, u_c in the figures is defined in Fig. 2. It is observed that the

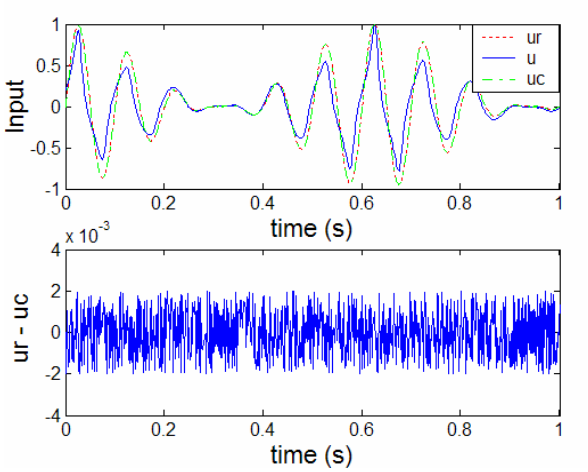

Fig. 9. Hysteresis compensation and compensation error

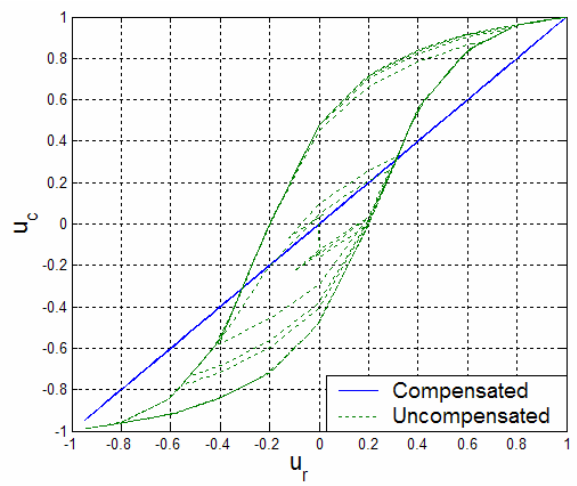

Fig. 10. Linearization of the hysteresis nonlinearity

compensation error $\left|u_r - u_c\right| \le \varepsilon$ where the threshold ε is set to 0.2% of the input range in this example. Fig. 10 shows that the relationship between the reference input u_r and the virtual input u_c to the linear component G of the plant with hysteresis nonlinearity is almost linear when the compensation of CNIA is applied.

IV. Closed-Loop Implementation

Although the time-optimal command is an open loop signal, it can be easily incorporated into a closed-loop framework as illustrated in Fig. 11. If the reference model G_0 is identical to the actual plant G and H^{-1} cancels H perfectly, the tracking error $e = 0$ and the resulting closed-loop response will be identical to the original open loop response. Otherwise the feedback controller C will modify the actual control input u to compensate for modeling errors. The only requirement is that the maximum allowable actuator limit for the time-optimal command be less than the actual actuator limit so that some actuator effort is available for the feedback control.

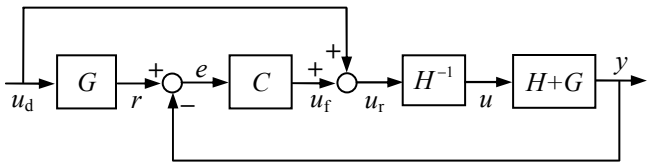

Fig. 11. Closed-loop implementation framework

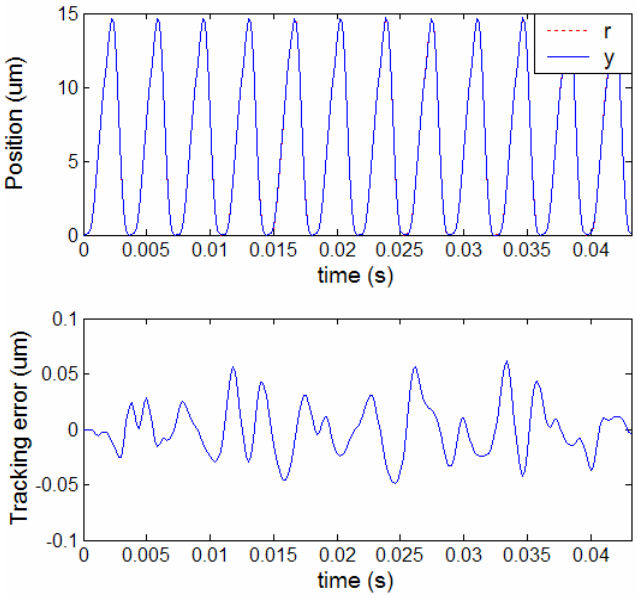

Fig. 12. Closed-loop implementation on the STM model with the hysteresis nonlinearity

Fig. 12 illustrates the closed-loop response obtained by incorporating the shaped command input, a 5th-order feedback controller by pole-placement, and the hysteresis compensation using CNIA whose convergence threshold is set to 2 mV. It can be observed that the uncertainty due to the hysteresis inversion error has been taken care of by the feedback compensation, while in the open loop case, the tracking error due to this uncertainty is as large as 0.2 μm .

V. Conclusion

This paper introduced a practical high-speed, high-precision motion control strategy for scanning of piezo-actuators used in scanning tunneling microscopy. The time-optimal feedforward input was obtained using the command shaping technique of constrained least-square optimization, and the hysteresis nonlinearity in the plant was compensated using the proposed continuous numerical inversion algorithm. Simulations were done and the high performance of the proposed controller was demonstrated. Future work includes experimental test on an actual piezo-actuator and study of the combined feedforward/feedback tracking strategy.

Acknowledgment

The author would like to thank his fellow Ph.D. student Michael C. Reynolds, who has by now graduated and become a faculty member at University of Arkansas, Fort Smith, for his many constructive and insightful comments.

References

[1] H. Perez, Q. Zou, and S. Devasia, "Design and control of optimal feedforward trajectories for scanners: STM example," Proceedings of the American Control Conference, May 2002, pp. 2305-2312.

[2] D. Croft, G. Shedd, and S. Devasia, "Creep, hysteresis, and vibration compensation for piezo-actuators: atomic force microscopy application," Proceedings of the American Control Conference, June 2000, pp. 2123-2128.

[3] D. Croft, and S. Devasia, "Vibration compensation for high speed scanning tunneling microscopy," Review of Scientific Instruments, Vol. 70, No. 12, December 1999, pp. 4600-4605.

[4] S. Salapaka, A. Sebastian, J.P. Cleveland, and M.V. Salapaka, "Design, identification and control of a fast nanopositioning device," Proceedings of the American Control Conference, May 2002, pp. 1966-1971.

[5] G. Schitter, P. Menold, H.F. Knapp, F. Allgoewer, and A. Stemmer, "High performance feedback for fast scanning atomic force microscopy," Review of Scientific Instruments, Vol. 72, No. 8, August 2001, pp. 3320-3327.

[6] X. Tan, and J.S. Baras, "A robust control framework for smart actuators," Proceedings of the American Control Conference, June 2003, pp. 4645-4650.

[7] C. J. Li, H.S.M. Beigi, S. Li, and J. Liang, "Nonlinear piezo-actuator control by learning self-tuning regulator," Transactions of the ASME, Vol. 115, December 1993, pp. 720-723.

[8] M.C. Reynolds, and P. Meckl, "The applica-tion of command shaping to the tracking problem," Proceedings of the American Control Conference, June 2003, pp. 3148-3153.

[9] I.D. Mayergoyz. *Mathematical Models of Hysteresis*. Springer-Verlag, New York, 1991.

[10] I.D. Mayergoyz, and G. Friedman, "Generalized Preisach model of hysteresis," IEEE Transactions on Magnetics, Vol. 24, No. 1, Jan. 1988, pp. 212-217.

[11] G. Tao, and P.V. Kokotovic. *Adaptive control of systems with actuator and sensor nonlinearities*. Wiley, 1996.

[12] D. Hughes, J.T. Wen, "Preisach modeling and compensation for smart material hysteresis," in Active Materials and Smart Structures, Proceedings of SPIE, Vol. 2427, 1994, pp. 50-64.

[13] R. Venkataraman, P. S. Krishnaprasad, "Approximate inversion of hysteresis: theory and numerical results," Proceedings of the 39th IEEE Conference on Decision and Control, 2000, pp. 4448-4454.

[14] X. Tan, R. Venkataraman, and P. S. Krishnaprasad, "Control of hysteresis: theory and experimental results," in Modeling, Signal Processing, and Control in Smart Structures, Proceedings of SPIE, Vol. 4326, 2001, pp. 101-112.

[15] L. Y. Pao, "Minimum-time control characteristics of flexible structures," Journal of Guidance, Control, and Dynamics, Vol. 19, No. 1, January-February 1996, pp. 123-129.